

Electrocodeposition of Nanocomposite Films

Jan B. Talbot

*Chemical Engineering Program
University of California, San Diego
La Jolla, CA*

Electrocodeposition is the process of particle incorporation during the electrodeposition of metal, producing metal matrix composite films. The electrocodeposition of nanometer-sized alumina particles in a copper matrix was systematically studied using a concentric cylindrical electrode (RCE) configuration. This electrode set-up allows the effects of hydrodynamics on particle incorporation to be investigated, with films that can be deposited either on the interior rotating or outer stationary cylinder. The deposition experiments were conducted with 50 nm diameter alumina particles as a function of particle size, solids loading, bath composition, electrode rotational rate, and current density up to mass transfer limited conditions. Gradient films have been made and also the effects of particle incorporation on the microstructure have been investigated. Recently, electrocodeposition of titania in nickel has been studied.

For more information contact:
Jan B. Talbot
Chemical Engineering Program
University of California, San Diego
La Jolla, CA 92093-0411
Phone - 858-534-3176
E-mail - jtalbot@ucsd.edu

Electrocodeposition is the process of particle incorporation during the electrolytic deposition of metal, as shown schematically in Fig. 1. This process has produced metallic matrix composite films containing particles of pure metals, ceramics, and organic materials, ranging in size from ~20 nm to 100 μm in diameter, embedded in electroplated Cu, Ni, Co, Cr, and various alloys. The concentration of particles suspended in solution has varied from 2 up to 200 g/L producing composites with typically 1-10 vol% of embedded particles¹⁻⁵; except when gravity settling was used where up to 50 vol% incorporation has been reported.⁶ Recently, impinging jet electrodeposition has produced an incorporation of up to 30 vol% SiC in a nickel matrix.⁷ Electrocodeposition plays an important role in many technological areas, such as transportation, construction, power generation and aerospace. The specific applications include surface coatings for cutting tools,⁸ high thermal-conductive dispersion-strengthening of materials for actively-cooled structures,⁹ high surface area electrodes for electrocatalysis in solar energy conversion and hazardous waste treatment,¹⁰ lubrication of surfaces,¹¹ and wear resistance in aircraft engines.¹² The advantages of composite electrodeposition over other coating methods are the uniformity of deposition even for complex shapes, reduction of waste often encountered in dipping or spraying techniques, low levels of contamination, the ability to produce functionally-gradient material and to continuously process parts. In addition, this process avoids the problems associated with high temperature and high pressure processing.

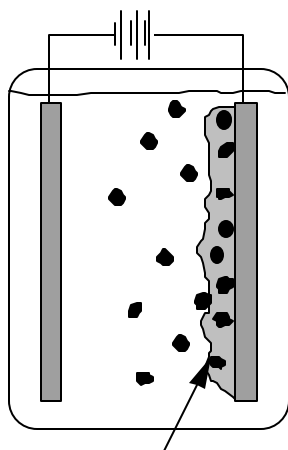


Fig. 1 Schematic of the electrocodeposition process.

Several review papers regarding electrocodeposition have been published over the years.^{1, 13-17} Recently, an update on experimental trends, mechanisms, and models in the literature was reported by Stojak, Fransaer and Talbot.¹⁸ From the research on electrocodeposition to date, a number of variables appear to be influential in the process, which include hydrodynamics, current density, particle characteristics, bath composition, and the particle-bath interaction. The influence that a particular variable has on the process is typically assessed by the change in the amount of particle incorporation obtained when that variable is adjusted. The effects of the process variables, of which many are interrelated, can vary for different particle-electrolyte

systems and electrodeposition cell configurations (such as parallel plates, rotating electrode, and impinging jet) with varying fluid flow and particle suspension.

Metallic matrix nanocomposites are of increasing interest due to their unique mechanical, magnetic and optical properties. The availability of a wide variety of nanosized particles and the ability to electrodeposit them in a metallic matrix with grain size of nanometer scale¹⁹ offers the potential of producing new materials for many novel applications. Actually, nanocomposites have been made by electrocodeposition since the 1970s, particularly Cu-Al₂O₃ as the electroplating of copper, particularly from acidic copper sulfate baths, is simple with ~100% current efficiency and alumina is readily available in monodispersed sizes. Table 1 compares the particle incorporation reported in the literature for parallel plate electrodes, rotating disk electrode (RDE) and rotating cylinder electrode (RCE) configurations for 50 nm-avg. diameter Al₂O₃ in copper. While alpha alumina has been observed to readily electrodeposit into copper films,^{2, 20-22} the ability to codeposit gamma alumina has been debated. Several researchers found that gamma alumina failed to codeposit with copper at all, independent of particle size from 20 to 300 nm.^{20, 21} Even in the cases where gamma alumina has been incorporated, the amount is about 10 times less than the amount obtained with the alpha phase,^{2, 22, 23} except for RCE results. From our RCE experiments at 1500 rpm and 158 g/L loading of particles in suspension, 4.4 wt% of alumina particles was incorporated,²⁴ which is more than three times the previously reported maximum amount of gamma alumina incorporation of 1.45 wt%.² Recently, pulse-reverse electrodeposition with an RCE was used to codeposit up to 14.6 wt% alumina particles, 30 nm in diameter, into a copper matrix, from suspensions where the particle diameters exceeded 150 nm.²⁶ The pulse-reverse method was selective for smaller particles independent of the electrolyte convection and, additionally, resulted in a higher particle incorporation compared to direct current (DC) deposition.

Other nanocomposites which have been produced by electrocodeposition are Ni-CdS, Ni-TiO₂, Ni-Al₂O₃, Ni-SiC, and Zn-SiO₂. Rajeshwar's group has prepared and characterized the photoelectrochemical behavior of nanocomposite films of CdS and TiO₂ (4.6 wt%) in a nickel matrix.^{10, 27, 28} These nanocomposite semiconductor films have shown enhanced photocurrent and a high selectivity. Ferkel and coworkers have investigated the electrodeposition of 14 nm avg. diameter Al₂O₃ particles in Ni with up to 4 vol% incorporated^{29, 30} and more recently, 25 nm Al₂O₃ using pulsed DC electroplating which yielded a preferential incorporation of smaller particles.³¹ Using a RCE, 0.14 to 1.03 wt% of 32 nm alumina was codeposited in nickel, with a larger amount of incorporation with increasing applied current density.³² Pulse-reverse plating with an RCE enhanced the alumina incorporation compared to DC plating in nickel.³² For example, at a duty cycle of 0.4, the alumina increased from 1.68 wt% for DC plating to 4.7 wt%. Pulse-reverse deposits had larger nodular microstructures than DC plated deposits. Searson et al.^{33, 34} electrocodeposited 50 and 300 nm Al₂O₃ particles in nickel films, which exhibited considerable enhancements in hardness in comparison to pure nickel with approximately 10–20 vol% incorporation using a RDE. Recently, they developed a model for the rate of nanometer-size particle incorporation into a growing film that takes into account the convective diffusion of particles to the surface and gravitational force, by treating particle incorporation in terms of the residence time at the surface.³⁴ The gravitational force was shown to be important for the codeposition of the 300 nm particles, but negligible for the 50 nm particles.

Table 1. Summary of Cu - 50 nm dia. Al₂O₃ codeposition results from the literature

Bath Composition	Electrode System	Particle Loading (g/L)	Current Density (mA/cm ²)	Analytical Method	Codeposition Results (wt%)*
250 g/L CuSO ₄ pH 1.0-3.0	Parallel	30	40	gravimetric	No incorporation ²⁰
120 g/L CuSO ₄ 100 g/L H ₂ SO ₄	Parallel	30	10-40	gravimetric	No incorporation ²¹
30 g/L CuSO ₄ pH 0.3	Parallel	20	5-15	atomic absorption	0.05 - 0.2 increase with current ²²
120 g/L CuSO ₄ 120 g/L H ₂ SO ₄	Parallel	5-20	5-70	atomic absorption	0.04 - 0.16 ² max at ~10 mA/cm ²
120 g/L CuSO ₄ 100 g/L H ₂ SO ₄	RDE	30	10-40	gravimetric	0.1 - 1.1 (decrease with flow ²¹
30 g/L CuSO ₄ 120 g/L H ₂ SO ₄	RDE	20	34	atomic absorption	0.03 - 0.055 max at 500 rpm from 255-1100 rpm ²³
30 g/L CuSO ₄ pH 0.3	RDE	20	10-80	atomic absorption	0.7 - 1.45 ² max at 20 mA/cm ²
0.1M CuSO ₄ 1.2M H ₂ SO ₄	RCE	39, 120, 158	5-90	electro-gravimetric	up to 4.4 ²⁴ () ²⁵ max at ~20 mA/cm ²
0.25M CuSO ₄ 0.3 M Citrate	RCE	12.5, 25	Pulse-reverse (PR) -5/+10	electron dispersive spectroscopy	DC 2.9, 3.5, 7.5 ²⁶ PR 6.8, 14.6, 12.7

* gamma-alumina unless indicated; 1 wt% = 2.9 vol% assuming a density of alumina of 3 g/cm³

Silicon carbide nanoparticles with a mean diameter of 20 nm were electrocodeposited into nickel up to 9 wt% (~25 vol%) using a RDE.³⁵ The incorporation of the SiC particles into nickel deposits was shown to modify the electrochemical impedance and cathodic polarization diagrams which correlated with the modification of the surface morphology and crystallinity of the nickel matrix. The pure nickel deposit had a regular surface, whereas the composite coating developed a nodular surface structure with a smaller nickel grain size. The incorporation mechanism of 50 nm SiO₂ particles electrocodeposited into zinc has been studied.³⁴

This paper will review our studies of the electrocodeposition of nanocomposites in which the effects of the bath solution and pH, the particle loading, and the hydrodynamics on the incorporation of 50 nm diameter alumina in copper were investigated using a RCE system.^{24, 25} Our investigations used the controlled hydrodynamics of the RCE system to provide a relatively uniform current density from kinetically controlled to the mass transfer influenced regions, resulting in a uniform electrodeposition rate and uniform particle shear rate at the electrode surface. Gradient films have been made and also the effects of particle incorporation on the surface morphology and microstructure have been investigated.³⁷ Recently, 300 nm diameter titania in nickel has been codeposited using the RCE.

Experimental Apparatus and Procedures

The RCE experimental apparatus and procedures for the electrocodeposition are described in detail elsewhere.^{24,25} The RCE was a Teflon shaft with a detachable, polished stainless steel cylindrical cathode machined to a height of 8 mm and a diameter of 12 mm with a total plating area of 3 cm². The concentric stationary anode was made from strips of copper foil with a total area of 13.6 cm²; the gap distance was 18 mm. The rotational rate of the RCE was controlled using an analytical rotator. To control and monitor the current and potential, a potentiostat/galvanostat and a host PC computer were used. After each experiment, the deposited film was carefully removed from the RCE.

The copper plating solution was 1.2M H₂SO₄ + 0.1M CuSO₄. Codeposition experiments were conducted using 50 nm alumina particles with loadings of 39 g/L (the minimum for analysis of incorporation), 120, and 158 g/L (the maximum to avoid settling), which corresponds to 1.2, 3.5, and 4.6 vol% of particles suspended in the electrolyte at room temperature. The amount of particle incorporation in copper was determined by an electrogravimetric analysis.²⁵ The typical weight of the codeposited films was 0.1 g, resulting in an accuracy in the particle incorporation of ±0.2 wt%. This technique was used for a film thickness of 15 μm. The amounts of particle incorporation for a least three experiments for each parameter set were within ±0.5 wt%. For gradient films 50 nm and also 3.0 μm alumina particles were used with a particle loading of 120 g/L and rotational rate of the RCE set at 1000 rpm. Additional mixing with a magnetic stir bar at ~80 rpm and in the direction cocurrently with the RCE was used with the 3 μm particles to prevent settling. The electrodepositions were performed galvanostatically with a current density ranging from 3 to 35 mA/cm². A scanning electron microscope (SEM) was used to observe the surface morphology of the deposited films.

For the electrocodeposition experiments for Ni-titania, a Watts plating bath containing approximately 200 g/L NiSO₄·6H₂O, 35 g/L NiCl₂·6H₂O, 30 g/L H₃BO₃ and 0.5 g/L sodium dodecyl sulphate (CH₃(CH₂)₁₁OSO₃Na) was used with a pH of 3.5-4.0 at either room temperature, 35-40 °C or 56 °C.³⁹ The bath contained either 40 g/L of 300 nm or 60 and 150 g/L of 5 μm avg. diameter TiO₂ powder. Current densities were in the range of 20-300 mA/cm². A SEM with an energy dispersive spectroscopy (EDS) was used for the study of surface morphology of deposits and for chemical analysis with an average accuracy of ±1 wt%.

Results and Discussion

Copper-Alumina Nanocomposites

The results of our electrocodeposition experiments for Cu-Al₂O₃ have been reported and discussed in detail elsewhere^{24, 25} and will be summarized here. Our study of the electrodeposition of Cu-Al₂O₃ nanocomposites was somewhat fortuitous. In order to understand the relationship between particle loading in suspension and the incorporation in a deposit, stability of the suspension was necessary. Of course, it was easiest to suspend the smallest particles; thus, the smallest particle available, 50 nm alumina, was used at a particle loading of 158 g/L or below to prevent settling. Nanosized particles tend to agglomerate; it was observed that in the dry state 50 nm particles agglomerated into particles of approximately 10 times the size of the individual particles. An advantage of the RCE was that the powders dispersed in solution separated under the shearing force of the rotating electrode into individual 50 nm

diameter particles, which are then incorporated into the electrodeposited film. Hence, experiments were conducted at RCE speeds of 500, 1000, and 1500 rpm over a range of current densities from 5 to 90% of limiting current. At a particle loading in suspension of 39 g/L, the amount of particle incorporation obtained at 1500 rpm for a range of current densities was about 0.5 wt%. The amount of codeposition increased with increasing particle loading for all the current densities evaluated at 1500 rpm. The 4.4 wt% of gamma alumina particle incorporation (158 g/L loading of particles in suspension) is more than three times the previously reported maximum amount of gamma alumina incorporation of 1.45 wt%.²

The crystallographic phase and the method used to manufacture the alumina powders were found to have a significant effect on incorporation. Powders, which were predominately gamma, had more than three times by volume the incorporation levels obtained with alpha alumina. Determination of the phase of the powders and identification of the processing method were necessary as the phase was not always as reported by the manufacturer.

The size (from 50 nm to 3 μm) and density differences of the alumina powders evaluated were found to have relatively little effect on codeposition. However, the particle loading in suspension is important. At low loadings, codeposition is limited by the supply of particles to the electrode. As the particle loading increases, so does the incorporation level. But at the highest loadings (beyond which powder settling becomes significant), the increase in incorporation is not proportional to the increase in loading.

The effect of hydrodynamics becomes clearer when the current density is normalized with the limiting current density, as shown in Fig. 2. The limiting current density for a RCE has shown to be proportional to the rotational rate raised to the 0.7 power.⁴⁰ Particle incorporation increases with current density for all rotational rates and particle loadings in suspension until about 20-25% of the limiting current density. In this region, the rate-determining step for codeposition appears to be the reduction of metallic ions adsorbed onto the alumina particles.

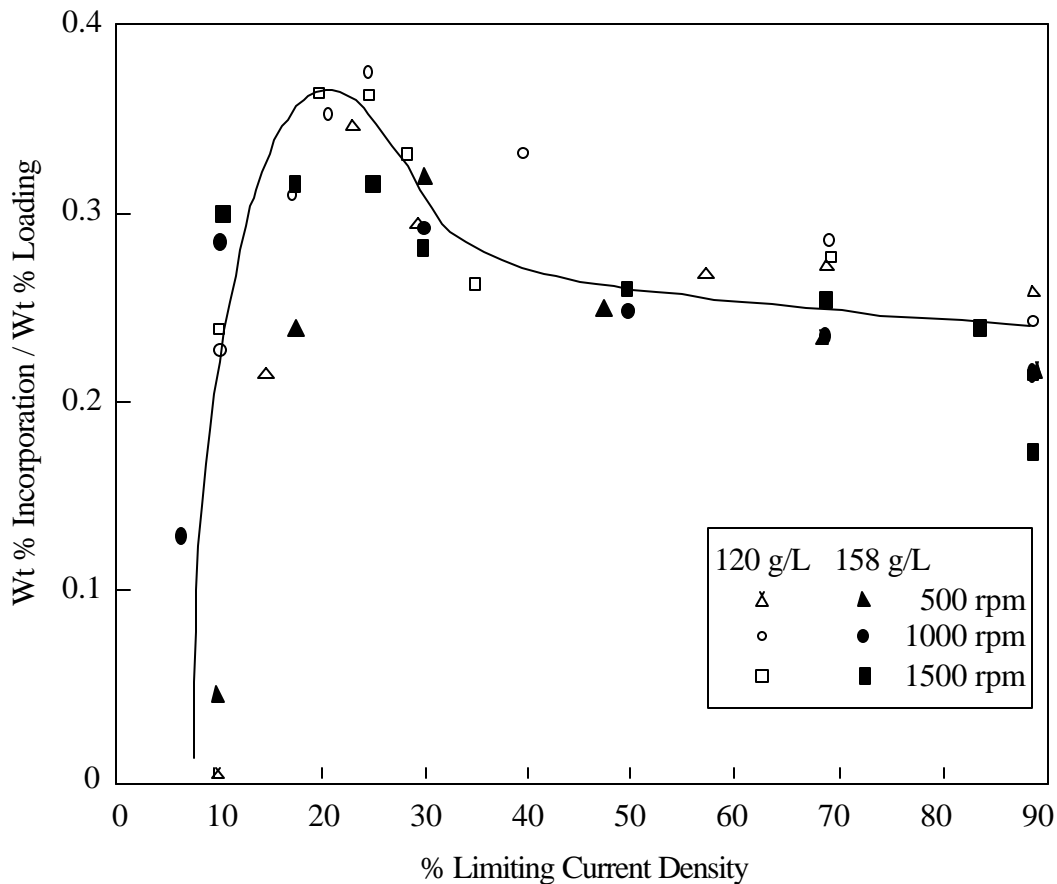


Fig. 2 Normalized particle incorporation vs. percent limiting current density as a function of RCE rotational rate at 120 g/L particle loading.

Then incorporation decreases with an increasing rate of metal deposition, then remains relatively constant until about 90% of the limiting current density when incorporation drops significantly. The regions wherein the amounts of incorporation sharply increase or decrease with current density are also more sensitive to particle size, and crystallographic phase. When the electrode polarity was changed, the particle incorporation results were similar to the results obtained using the rotating cylinder as the cathode. With a stationary cathode, incorporation increased with increasing current density to a maximum at about 15% of the limiting current density.

The most influential process parameter on the resulting particle incorporation (as long as there is a sufficient particle loading in suspension) appears to be the percentage of limiting current density, which inherently involves the system hydrodynamics and overpotential. The relative effects of other process variables can be evaluated more clearly when related to the percentage of limiting current density.

Gradient Films

With a "particle incorporation map" as shown in Fig. 2 and one similarly collected for 3 μm dia. alumina particles in copper using a RCE system,³⁶ gradient films were produced. The maps are similar as shown in Fig. 3, except that the maximum particle incorporation increased from 4 to 5 wt% (at 5 mA/cm^2) with an increase in particle size from 50 nm to 3 μm . A specified amount of particles codeposited was achieved by varying either current density or bath mixing. It was found that gradients that were plated using alternating current densities had approximately the same particle incorporation as films plated with the same current density throughout.

The surface morphology of uniform and gradient films was studied, mainly for films of copper with 3 μm dia. alumina particles.^{37,38} The effects of particle incorporation, particle size, and current density on surface morphology were studied from SEM micrographs of 15 μm thick films and four (each 15 μm thick) layered graded films. The effect of particle size on the surface morphology is illustrated by comparing the surfaces of a four layered film with 3 μm particles to that with 50 nm particles in Fig. 4 plated at 35 mA/cm^2 with approximately 3 wt% and 1 wt% incorporated, respectively. The defined nodules observed for the film with 3 μm particles are barely apparent in the film with 50 nm particles incorporated. There is a decrease in the size of the nodules as well as a loss of definition with incorporation of the smaller size particles. The smaller particles may allow for the diffusion of the copper adatoms across the smaller surfaces of the particles.

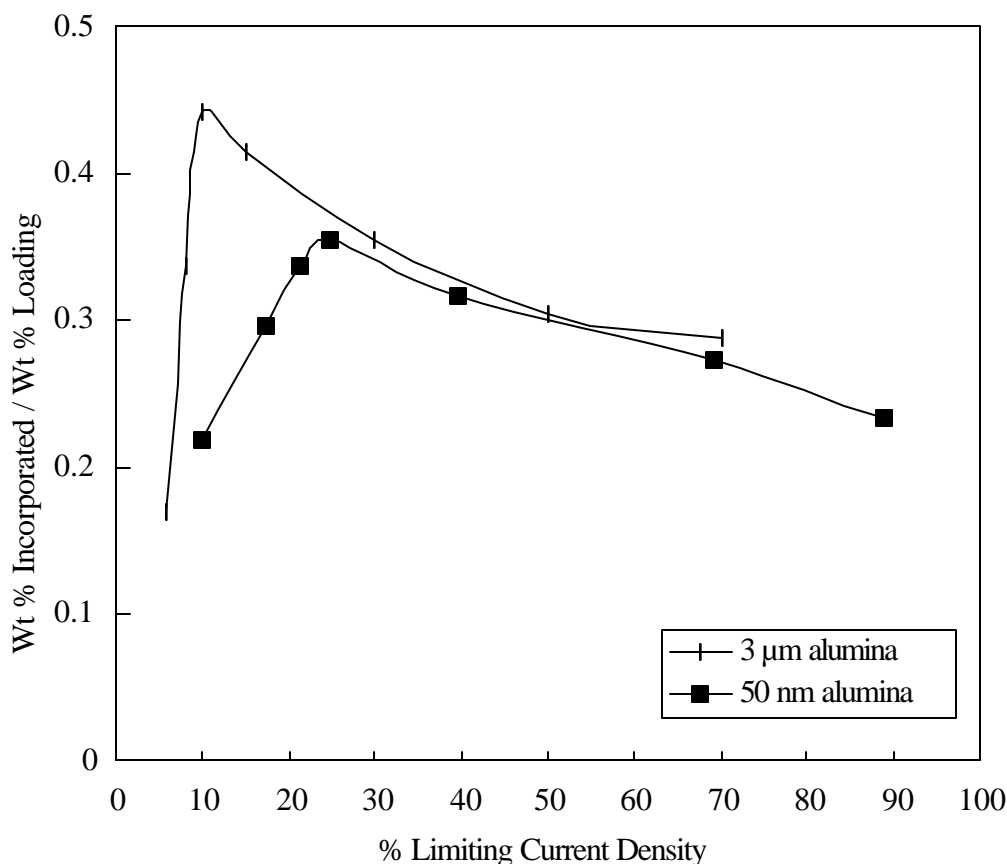


Fig.3 Comparison of particle incorporation for 3 μm and 50 nm alumina particles (120 g/L at 1000 rpm).

Nickel-Titania Nanocomposites

A preliminary study of the electrocodeposition of Ni-TiO₂ composite films was performed with two different average sizes of particles, $\sim 5 \mu\text{m}$ ³⁹ and 300 nm with various particle loadings and current densities. The experiments with 5 μm particles were conducted at RCE speeds of 500, 1000, and 1500 rpm with a range of current densities from 30-180 mA/cm². The experiments with 300 nm particles were performed at a rotational rate of 1000 rpm with two different current density ranges of a low range of 30-80 mA/cm² and a high range of 220-300 mA/cm². The current efficiencies ranged from 98-99.5%. The films deposited from baths which contained 10 g/L of 5 μm TiO₂ did not contain any TiO₂ at any current density and cathode rotational speed. However, titania particles were incorporated from higher bath loadings. The maximum amount of incorporation was 7 wt% for the 5 μm particles and 4.3 wt% for the 300 nm particles. The amount of 5 μm titania codeposited with nickel is much higher than the incorporation of alumina in copper with the RCE. The normalized particle incorporation as a function of percent limiting current density in Fig. 5 presents all of the Ni-TiO₂ data. As compared to the graph for Cu-alumina deposits in Fig. 2, the ratio of wt% incorporation/wt% loading is much greater for both the 5 μm and 300 nm titania particles in nickel. Although there is much more uncertainty in the incorporation data for Ni-TiO₂ (due to both not repeating experiments and from inaccuracy of

analysis by EDS), these preliminary results indicate similar trends in particle incorporation with a monotonic increase in the amount of particles with increasing current density with a maximum at 15-20 % of limiting current density and a decrease in incorporation at higher current densities. There seemed little effect of bath temperature or particle loadings of 40 g/L or greater. It is difficult to determine if there is an effect of particle size.

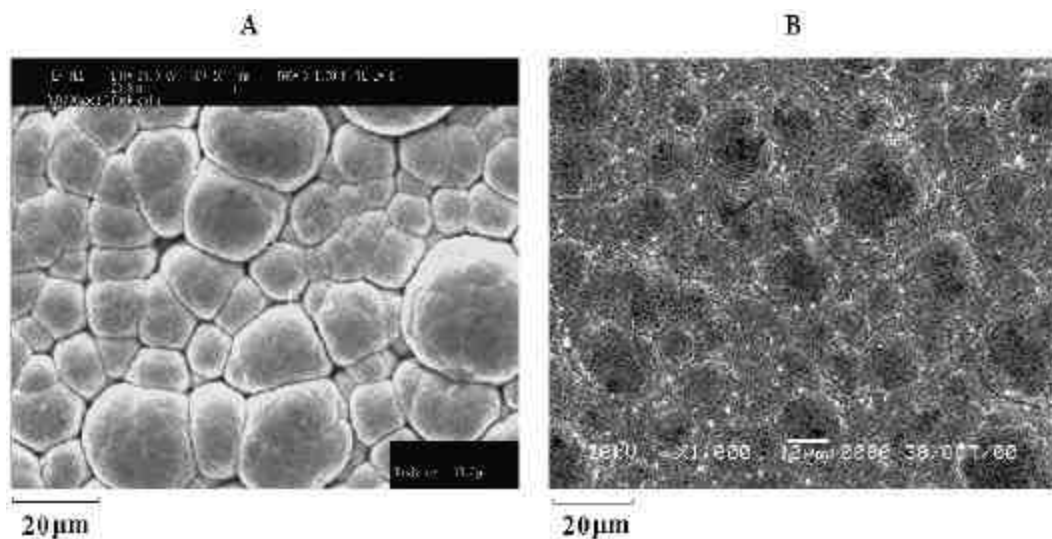


Fig. 4. Comparison of micrographs of the surfaces of 60 μm thick films at 35 mA/cm^2 : (A) with four 15 μm layers with ~ 3 wt% of 3 μm particles and (B) with four 15 μm layers with each 1.0 wt% of 50 nm particles.

The surface morphologies of the codeposited films show globular grains which are generally smaller with the smaller size titania particles. With 300 nm titania particles, it was observed that the films deposited in the high current density range had smaller grains than the films produced at lower current densities.⁴⁰

Conclusions

The RCE has provided a controllable, reproducible experimental system to study the electrocodeposition process, which has been particularly useful for producing nanocomposites. The RCE system provides particle suspension, uniform current distribution, and uniform particle shear rate at the electrode surface over a range of deposition conditions from kinetically to mass-transfer control. The ability to measure particle incorporation accurately is important. For $\text{Cu}-\text{Al}_2\text{O}_3$ composites, an electrogravimetric method proved very accurate at ± 0.5 wt%; however, this method was not found usable for the $\text{Ni}-\text{TiO}_2$, so that EDS was used.³⁹ The process variables evaluated included: electrode rotational rate, current density (5 to 90% of limiting current density), particle loading, and particle size. The particle loading in suspension must be optimized to be above a minimum amount to yield composites (which is limited by the detection level of the analytical method used) and below an amount where settling of particles occurs. Another advantage of the RCE is that agglomerated particles are separated under the shearing force of the rotating electrode, which are then incorporated into the electrodeposited film.

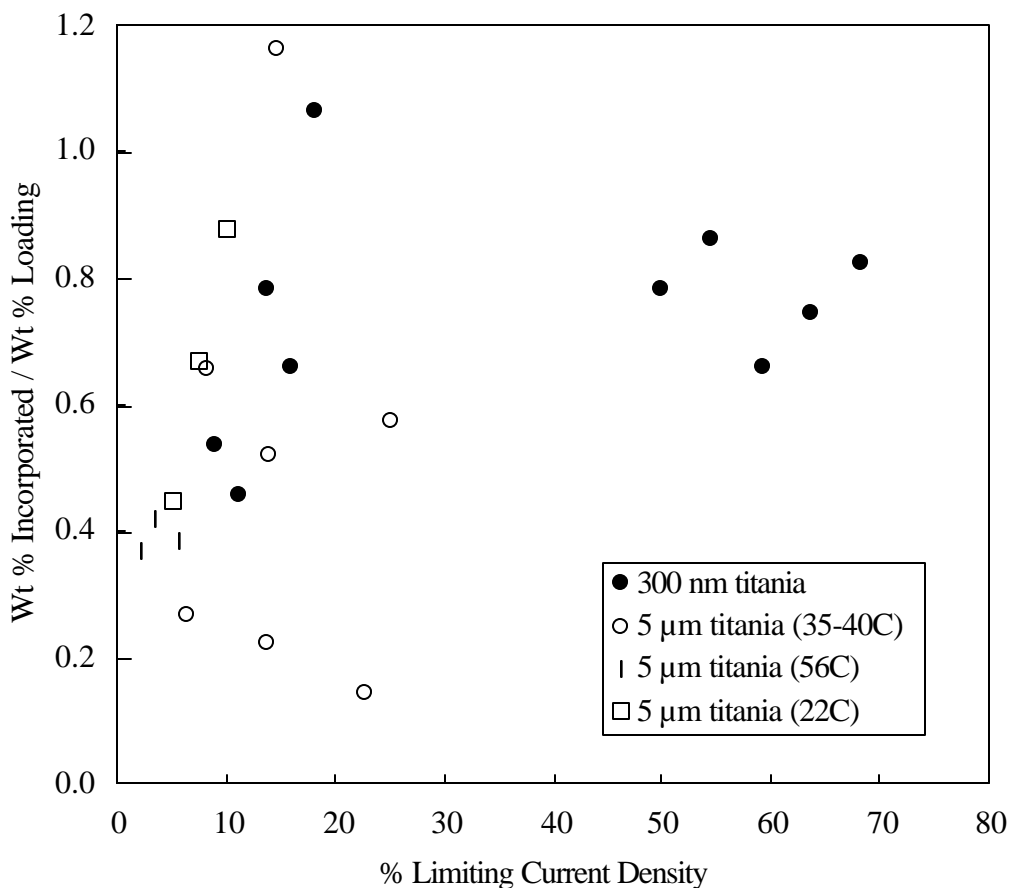


Fig.5 Comparison of particle incorporation for 5 μm and 300 nm titania particles in nickel.

With the RCE, the maximum amount of incorporation of 4.4 wt% alumina in copper for 158 g/L loading of particles in suspension is approximately 40 times the amount of incorporation (or 3 times for vol% loading) reported in the literature previously. The preliminary results of electrocodeposition of Ni-TiO₂ show a high incorporation of 7 wt% for the 5 μm particles and 4.3 wt% for the 300 nm particles. The electrocodeposition data can be readily compared by normalizing the wt% particle incorporation with the particle loading and plotting the results versus percent limiting current density. It was shown that is an increase in particle incorporation in the kinetically-controlled regime, reaching a maximum incorporation at 15-25% of limiting current density. Then incorporation decreases and finally levels off during ohmic control, until mass transfer effects cause a sudden decrease. The effects of the hydrodynamics are also normalized by presenting the data in terms of percent limiting current density, which is dependent on rotational rate.

Using the particle incorporation maps, gradient films of Cu-Al₂O₃ composites were easily produced. The surface morphology of uniform and gradient films was studied. It was found that there is an increase in the number of nodules per surface area (reduction of individual nodules)

due to particle incorporation. In addition, with a decrease in the incorporated particle size, there was a decrease in the nodule size as well as a loss in definition, where the boundaries become less apparent. For gradient films, the surface morphology of the previous layers in the deposition do not significantly alter the surface morphology at a particular current density, provided that the thickness of the layer is large enough for the morphology to develop. Also, similar particle incorporation in a film but with different surface morphology can be achieved by plating either in the kinetically controlled or mass transfer influenced region.

Although the RCE system has allowed for a systematic study of the electrocodeposition process, a deposit onto a cylinder is not often practical for industrial applications. Future research will be performed using an impinging jet electrodeposition set-up. This configuration will allow for significantly higher limiting current densities leading to increased deposition rates, with the ability to study the effects of controlled hydrodynamics on particle incorporation, but on a flat substrate. Recently, composites of Ni-Al₂O₃⁴² and compositionally-graded Ni-P deposits containing SiC particles⁷ were obtained using jet electroplating. The amount of SiC particles incorporated in the deposit could be controlled by the electrolyte jet velocity; the incorporation increased from 0 to 30 vol% as the jet velocity decreased from 16 to 0.5 m/s.⁷ The impinging jet electrode configuration should allow for a method of creating homogenous or gradient nanocomposite films at fast rates to accommodate a wide range of processing conditions.

Acknowledgements

The research was supported in part by the National Science Foundation. The author thanks Dr. Jean Stojak, David Wang, and Adam Stolen who performed the research as part of their graduate degree programs. Most of titania-nickel electrocodeposition research was performed by Dr. M.E. Bahrololoom during his sabbatical leave from Shiraz University, Shiraz, Iran.

References

1. V.P. Greco, *Plating and Surface Finishing*, **76(7)**, 62 (1989); **76(10)**, 68 (1989).
2. J.R. Roos, J.P. Celis, & J.A. Hansen, *Trans. Inst. Metal Finishing*, **55**, 113 (1977).
3. C. White & J. Foster, *Trans. Inst. Metal Finishing*, **59**, 9 (1981).
4. S.W. Watson & R.P. Walters, *J. Electrochem. Soc.*, **138**, 3633 (1991).
5. P.R. Webb & N.L. Robertson, *J. Electrochem. Soc.*, **141**, 669 (1994).
6. M. Ghouse, M. Viswanathan, & E.G. Ramachadran, *Metal Finishing*, **78**, 55 (1980).
7. H. Takeuchi, Y. Tsunekawa, & M. Okumiya, *Materials Transactions, JIM*, **38(1)**, 43 (1997).
8. G.A. Malone, *Plat. Surf. Finish.*, **78**, 58 (1991).
9. J.R. Groza & J.C. Gibeling, *Mater. Sci. Eng.*, **A171**, 115 (1993).
10. N.R. de Tacconi, H. Wenren, & K. Rajeshwar, *J. Electrochem. Soc.*, **144(9)**, 3159 (1997).
11. H. Abi-Akar, C. Riley, & G. Maybee, *Chem. Mater.*, **8(11)**, 2601 (1996).
12. E.C. Kedward & K.W. Wright, *Plat. Surf. Finish.*, **65**, 38 (1978).
13. R.V. Williams, *Electroplating and Metal Finishing*, **3**, 92 (1966).
14. E. C. Kedward, *Cobalt*, **3**, 53 (1973).
15. J. R. Roos, J. P. Celis, J. Fransaer, & C. Buelens, *J. Metals*, **42**, 60 (1990).
16. J. Fransaer, J. P. Celis, & J. R. Roos, *Metal Finishing*, **91**, 97 (1993).

17. A. Hovestad & L.J.J. Janssen, *J. Appl. Electrochem.*, **40**, 519 (1995).
18. J. L. Stojak, J. Fransaer & J.B. Talbot, in *Advances in Electrochemical Science and Engineering*, R.C. Alkire and D. M. Kolb (Eds), Vol 7, Wiley-VCH, Weinheim, Germany, 2002; p. 193.
19. G. Palumbo, F. Gonzalez, K. Tomantschger, U. Erb, & K.T. Aust, *Plating and Surface Finishing*, **90(2)**, 36 (2003).
20. E. S. Chen, G. R. Lakshminarayanan, & F. K. Sautter, *Metal. Trans.*, **2**, 937 (1971).
21. C. C. Lee & C. C. Wan, *J. Electrochem. Soc.*, **135**, 1930 (1988).
22. J. P. Celis, J. R. Roos, & C. Buelens, *J. Electrochem. Soc.*, **134**, 1402 (1987).
23. C. Buelens, J. P. Celis, & J. R. Roos, *J. Appl. Electrochem.* **13**, 541 (1983).
24. J. L. Stojak & J. B. Talbot, *J. Electrochem. Soc.*, **146(12)**, 4504 (1999).
25. J. L. Stojak, Ph.D. thesis, University of California, San Diego (1997).
26. E.J. Podhala, *Nanoletters*, **1(8)**, 413 (2001).
27. M. Zhou, W.-Y. Lin, N. R. de Tacconi, & K. Rajeshwar, *J. Electroanal. Chem.*, **402**, 221 (1996).
28. M. Zhou, N. R. de Tacconi, & K. Rajeshwar, *J. Electroanal. Chem.*, **421**, 111 (1997).
29. H. Ferkel, B. Muller, & W. Riehemann, *Mat. Sci. and Engineering*, **A234**, 474 (1997).
30. B. Muller & H. Ferkel, *Nanostruct. Mater.*, **10**, 1285 (1998).
31. J. Steinbach & H. Ferkel, *Scripta Mater.*, **44**, 1813 (2001).
32. A.B. Vidrine & E.J. Podhala, *J. Appl. Electrochem.*, **31**, 461, 2001.
33. R. R. Oberle, M. R. Scanlon, R. C. Cammarata, & P. C. Searson, *Appl. Phys. Lett.*, **66(1)**, 19 (1995).
34. P. M. Vereecken, I. Shao, & P. C. Searson, *J. Electrochem. Soc.*, **147(7)**, 2572 (2000).
35. L. Benea, P. L. Bonora, A. Borello, S. Martelli, F. Wenger, P. Ponthiaux, & J. Galland, *J. Electrochem. Soc.*, **148(7)**, C461 (2001).
36. K. Kondo, A. Ohgishi, & Z. Tanaka, *J. Electrochem. Soc.*, **147(7)**, 2611 (2000).
37. D.C Wang & J.B. Talbot, *The Electrochemical Society Softbound Proceedings*, Pennington, NJ (2001).
38. D. C. Wang, MS thesis, University of California, San Diego (2001).
39. A.C. Stolen, MS thesis, University of California, San Diego (2002).
40. M. Eisenberg, C. W. Tobias, & C. R. Wilke, *J. Electrochem. Soc.*, **101**, 306 (1954).
41. M. E Bahrololoom, A. C. Stolen, & J.B. Talbot, in preparation.
42. M. Okumiya, H. Takeuchi, and Y. Tsunekawa, *J. Japan Inst. Metals*, **59(6)**, 640 (1995).